ЖУРНАЛ СТРУКТУРНОЙ ХИМИИ

2015. Том 56, № 4 *Июль* *С. 764 – 772*

UDC 548.73:546.72:546.18:546.21

CRYSTAL STRUCTURE AND THERMAL STABILITY OF NEW IRON PHOSPHATES $KMFe(PO_4)_2$ (M = Ni, Mg, and Co)

A. Badri[1], M. Hidouri[1], M.L. López[2], M.L. Veiga[2], C. Pico[2], J. Darriet[3], M. Ben Amara[1]

[1]*UR Matériaux Inorganiques, Faculté des Sciences, Université de Monastir, Monastir, Tunisie*
E-mail: mongi.benamara@fsm.rnu.tn
[2]*Departamento de Química Inorgánica I, Facultad de Ciencias Químicas, Universidad Complutense, Madrid, Spain*
[3]*Institut de Chimie de la Matière Condensée de Bordeaux, CNRS, Université de Bordeaux I, Pessac-Cedex, France*

Received November, 4, 2013

Three isostructural iron monophosphates $KNiFe(PO_4)_2$ (KNi), $KMgFe(PO_4)_2$ (KMg-LT, where LT means "low-temperature stable phase"), and $KCoFe(PO_4)_2$ (KCo-LT) are synthesized and structurally characterized from X-ray diffraction data. They crystallize in the monoclinic system with the space group $P2_1/c$. Their structures have in common a three-dimensional framework, built up by infinite zigzag chains of edge-sharing MO_6 (M = Ni, Mg or Co) octahedra, linked by FeO_5 and PO_4 polyhedra via vertices and edges to form a rigid skeleton. The K^+ ions are located in formed tunnels. DTA showed that KNi has a congruent melting at 941 °C, whereas KMg-LT and KCo-LT undergo irreversible phase transitions from $P2_1/c$ to different high-temperature structures with the $C2/c$ symmetry. IR absorption bands are assigned to different vibrations of the PO_4 tetrahedron.

DOI: 10.15372/JSC20150415

K e y w o r d s: iron phosphates, synthesis, crystal structure, phase transitions, IR.

INTRODUCTION

Iron phosphate materials have received much attention over the past three decades because they have shown to be of a great interest both for their applications in many fields such as catalysis [1, 2], ionic conductivity [3], and as electrode materials for rechargeable batteries [4] and rich structural chemistry [5, 6].

As a part of our investigation on the A_2O—MO—Fe_2O_3—P_2O_5 systems, where A and M are alkali and divalent cations respectively, we reported the crystal structures and physical characterization of phosphates $KMgFe(PO_4)_2$ [7] and $KCuFe(PO_4)_2$ [8]. These two phases have similar stoichiometries, but very different structures. Indeed, magnesium phosphate displays a bi-dimensional structure, built up from layers of corner-sharing $(Fe,Mg)O_4$ and PO_4 tetrahedra, the K^+ cations being located within the interlayer space. By contrast, the structure of copper phosphate is three-dimensional, built up by crossing chains of Cu_2O_8 units, alternating with FeO_6 octahedra; the K^+ ions are found in one-dimensional hexagonal tunnels running along the [101] direction.

Recently, M.M. Yatskin et al. have reported the formation of three new compounds: $KMg_{0.09}Fe_{1.91}(PO_4)_2$ [9] and $KM^{II}Fe(PO_4)_2$ (M^{II} = Co, Ni) [10]. In addition, the structural characterization revealed that the first compound was isotypic with $KM^{II}Fe(PO_4)_2$ (M^{II} = Cu, Fe) [8, 11]. As a new contribution, in this work we present the structural determination from X-ray diffraction and the

characterization by DTA and IR spectroscopy of three isotypic iron phosphates $KMFe(PO_4)_2$ (M^{II} = Ni, Mg, Co). The nickel compound (abbreviated KNi) is thermally stable until its melting temperature of 941 °C. The magnesium one KMg-LT (low-temperature stable phase) exhibits an irreversible phase transition at 778 °C to the high-temperature stable phase with a lamellar structure, previously reported for phosphate $KMgFe(PO_4)_2$ [7]. The cobalt sample KCo-LT (low-temperature stable phase) also displays an irreversible phase transition at 843 °C to a high-temperature structure which is isotypic with phosphate $KCoAl(PO_4)_2$ [12].

EXPERIMENTAL

Synthesis. The title compounds were synthesized as single crystal phases by growing in a flux of potassium dimolybdate $K_2Mo_2O_7$, starting from KNO_3 (Fluka, 99 %), $M(NO_3)_2 \cdot 6H_2O$ (M = Mg, Co, Ni; Fluka, 99 %), $Fe(NO_3)_3 \cdot 9H_2O$ (Acros, 99 %), $(NH_4)_2HPO_4$ (Merck, 99 %), and MoO_3 (Acros, 99 %). These reactants were taken in the atomic ratio K:M:Fe:P:Mo = 2:1:1:2:1 for KNi and KCo and K:M:Fe:P:Mo = 2:1:1:2:2 for KMg-LT. Recall that in the case of Mg compound, the atomic ratio K:M:Fe:P:Mo = 2:1:1:2:1 led to the high-temperature variety with a lamellar structure [7]. For each compound, the weighted amounts were mixed via dissolving in aqueous nitric acid and the obtained solution was evaporated to dryness. The resulting dry residues were ground in an agate mortar to ensure their best homogeneity, and then gradually heated up to 873 K in a platinum crucible. After being reground, the mixture was melted at 1223 K for 1 h, then cooled down to 673 K at a rate of 10 $K \cdot h^{-1}$, and afterwards rapidly cooled to room temperature by switching off the furnace. The final products were washed with warm water in order to dissolve the flux.

The KNi compound was also obtained as a single polycrystalline phase by the conventional solid state reaction, starting from a stoichiometric mixture of KNO_3 (Fluka, 99 %), $Ni(NO_3)_2 \cdot 6H_2O$ (Fluka, 99 %), $Fe(NO_3)_3 \cdot 9H_2O$ (Acros, 99 %), $(NH_4)_2HPO_4$ (Merck, 99 %). After initial treatment similar to that performed for the synthesis of the single crystals until 873 K, the sample was subjected to final calcinations at 1143 K for 48 h with intervening grinding. A yellow-brown powder was obtained by quenching in air. Its purity was confirmed by its X-ray powder diagram (Fig. 1) collected in the range $9° \leq 2\theta° \leq 100°$ on a PANalytical diffractometer using CuKα radiation (λ = 1.5406 Å).

Structure determination. Data collection was performed on an Enraf-Nonius CAD4 diffractometer for KNi and KMg-LT and on a Bruker Nonius Kappa CCD diffractometer for KCo-LT, using monochromated MoK_α radiation (λ = 0.7107 Å). The three compounds crystallize in the monoclinic system with cell parameters listed in Table 1.

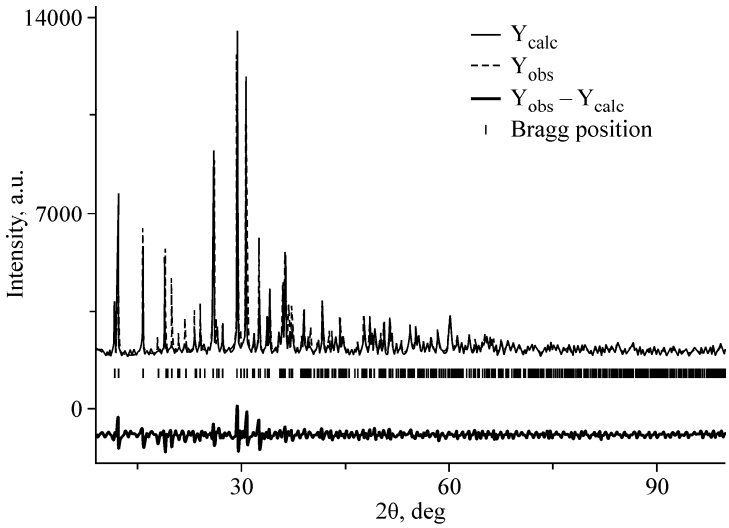

Fig. 1. Powder X-ray diffraction pattern for $KNiFe(PO_4)_2$

The systematic absences ($k = 2n$ for $0k0$ and $l = 2n$ for $h0l$) indicated the space group $P2_1/c$. The application of direct methods [13] allowed the location of the heavy atoms. Subsequently, the other atoms were progressively located from Fourier difference maps [14] after the refinement of the known atomic positions.

The refinement including anisotropic thermal parameters led to the final reliability factors $R_1 = 0.032$, $wR_2 = 0.080$, $S = 1.130$ for KNi, $R_1 = 0.029$, $wR_2 = 0.081$, $S = 1.089$ for KMg-LT, and $R_1 = 0.021$, $wR_2 = 0.048$, $S = 1.103$ for KCo-LT. Relevant crystallographic data and further details of the X-ray data collections and refinements are summarized in Table 1. The atomic coordinates are listed in Tables 2, 3, and 4 respectively.

Further details of the crystal structure investigations may be obtained from Fachinformationszentrum Karlsruhe, 76344 Eggen-stein-Leopoldshafen, Germany (fax: (+49)7247-808-666; e-mail: crys-

Table 1

Details of the data collections and structural refinements for $KMFe(PO_4)_2$ (M = Ni, Mg *and* Co)

	Crystal data		
Chemical formula	KNi	KMg-m	KCo-m
Crystal system	Monoclinic	Monoclinic	Monoclinic
Space group	$P2_1/c$	$P2_1/c$	$P2_1/c$
a, Å	5.101(2)	5.171(3)	5.148(1)
b, Å	14.456(2)	14.479(2)	14.403(2)
c, Å	9.216(1)	9.209(2)	9.256(1)
β, deg.	104.73(2)	105.02(1)	104.87(2)
Z	4	4	4
ρ_{cal}, g/cm^3	3.47	3.08	3.44
	Data collection		
Crystal dimensions, mm	0.1×0.16×0.3	0.12×0.18×0.4	0.13×0.2×0.3
Diffractometer	CAD4 (Enraf-Nonius)	CAD4 (Enraf-Nonius)	CCD (Nonius Kappa)
Radiation	$\lambda(MoK_\alpha) = 0.7107$Å	$\lambda(MoK_\alpha) = 0.7107$Å	$\lambda(MoK_\alpha) = 0.7107$Å
Monochromator	Graphite	Graphite	Graphite
μ, mm^{-1}	6.202	3.475	5.807
Scan type	ω/2θ	ω/2θ	ω/2θ
Scan speed	Variable	Variable	Variable
$2\theta_{max}$, deg.	59.9	59.9	80
Number of unique / observed reflections[$I > 2\sigma(I)$]; R_{int}	1907 / 1824; 0.062	2695 / 1829; 0.025	4105 / 3732; 0.000
Indices	$-1 \le h \le 7$, $-1 \le k \le 20$ $-12 \le l \le 12$	$-1 \le h \le 7$, $-1 \le k \le 20$ $-12 \le l \le 12$	$-9 \le h \le 9$, $0 \le k \le 26$ $0 \le l \le 16$
$F(000)$	668	604	664
	Structural refinement		
Intensity corrections	Lorentz-polarisation	Lorentz-polarisation	Lorentz-polarisation
Absorption correction ($T_{min, max}$)	Ψ-Scan (0.29, 0.43)	Ψ-Scan (0.49, 0.53)	Gaussian
Structure solution	Direct methods	Direct methods	Direct methods
Reliability factors	$R_1 = 0.032$; $wR_2 = 0.080$; $S = 1.130$	$R_1 = 0.029$; $wR_2 = 0.081$; $S = 1.089$	$R_1 = 0.021$; $wR_2 = 0.048$; $S = 1.103$
Number of parameters	119	119	119
$(\Delta\rho)_{max, min}$, e/Å^3	1.04, –1.33	0.95, –0.84	1.730, –1.424

Table 2

Atomic coordinates and equivalent thermal parameters U_{eq} (Å^2) *for* $KNiFe(PO_4)_2$

Atom	Wyckoff	$x(\sigma)$	$y(\sigma)$	$z(\sigma)$	$U_{eq}(\sigma)$
K	4*e*	0.8121(1)	0.3238(2)	0.1869(2)	0.0213(1)
Ni	4*e*	0.7572(2)	0.0451(1)	0.0387(3)	0.0061(1)
Fe	4*e*	0.2273(2)	0.1289(2)	0.3822(2)	0.0055(1)
P1	4*e*	0.2563(1)	0.1719(4)	0.0364(1)	0.0053(1)
O11	4*e*	0.1184(4)	0.2441(2)	0.4445(2)	0.0088(3)
O12	4*e*	0.2359(4)	0.1886(1)	0.1970(2)	0.0111(3)
O13	4*e*	0.0834(3)	0.0862(2)	–0.0321(2)	0.0072(3)
O14	4*e*	0.5500(4)	0.1646(2)	0.0291(2)	0.0108(3)
P2	4*e*	0.6919 (1)	0.0064(1)	0.3215(2)	0.0053(2)
O21	4*e*	0.4928(4)	–0.0129(3)	0.1708(2)	0.0098(3)
O22	4*e*	0.9438(4)	0.0478(3)	0.2757(2)	0.0091(3)
O23	4*e*	0.5861(4)	0.0792(3)	0.4138(2)	0.0092(3)
O24	4*e*	0.7753(4)	–0.0814(3)	0.4129(2)	0.0106(3)

Table 3

Atomic coordinates and equivalent thermal parameters U_{eq} (Å^2) *for* $KMgFe(PO_4)_2$

Atom	Wyckoff	$x(\sigma)$	$y(\sigma)$	$z(\sigma)$	$*U_{eq}(\sigma)$
K	4*e*	0.8234(1)	0.3233(4)	0.1803(2)	0.0199(1)
Mg	4*e*	0.7590(2)	0.0492(5)	0.0331(2)	0.0060(1)
Fe	4*e*	0.2263(6)	0.1282(2)	0.3829(1)	0.0060(1)
P1	4*e*	0.2556(1)	0.1731(4)	0.0372(2)	0.0051(2)
O11	4*e*	0.1158(3)	0.2433(1)	0.4449(3)	0.0091(3)
O12	4*e*	0.2339(4)	0.1891(1)	0.1981(3)	0.0120(3)
O13	4*e*	0.0876(3)	0.0869(1)	–0.0290(3)	0.0074(3)
O14	4*e*	0.5455(3)	0.1663(1)	0.0313(2)	0.0100(3)
P2	4*e*	0.6906(1)	0.0068(4)	0.3196(2)	0.0052(2)
O21	4*e*	0.4986(3)	–0.0126(1)	0.1668(3)	0.0098(3)
O22	4*e*	0.9396(3)	0.0486(2)	0.2767(3)	0.0094(3)
O23	4*e*	0.5811(3)	0.0785(1)	0.41079(19)	0.0096(3)
O24	4*e*	0.7704(3)	–0.0808(1)	0.41126(19)	0.0109(3)

Table 4

Atomic coordinates and equivalent thermal parameters U_{eq} (Å^2) *for* $KCoFe(PO_4)_2$

Atom	Wyckoff	$x(\sigma)$	$y(\sigma)$	$z(\sigma)$	$*U_{eq}(\sigma)$
K	4*e*	0.8202(1)	0.3254(2)	0.1842(1)	0.0209(1)
Co	4*e*	0.7554(3)	0.0479(1)	0.0363(1)	0.0074(3)
Fe	4*e*	0.2251(1)	0.1281(1)	0.3812(1)	0.0059(2)
P1	4*e*	0.2557(1)	0.1727(2)	0.0373(3)	0.0057(1)
O1	4*e*	0.1181(2)	0.2436(1)	0.4446(1)	0.0099(2)
O2	4*e*	0.2309(2)	0.1886(1)	0.1961(1)	0.0121(1)
O3	4*e*	0.0897(2)	0.0862(2)	–0.0313(1)	0.0079(1)
O4	4*e*	0.5477(1)	0.1662(1)	0.0327(1)	0.0116(1)
P2	4*e*	0.6899(1)	0.00703(2)	0.3237(3)	0.0058(1)
O11	4*e*	0.4894(2)	–0.0149(2)	0.1762(1)	0.0125(1)
O12	4*e*	0.9367(2)	0.0488(1)	0.2766(1)	0.0101(1)
O13	4*e*	0.5834(1)	0.0804(1)	0.4141(2)	0.0119(1)
O14	4*e*	0.7787(1)	–0.0797(1)	0.4167(2)	0.00697(14)

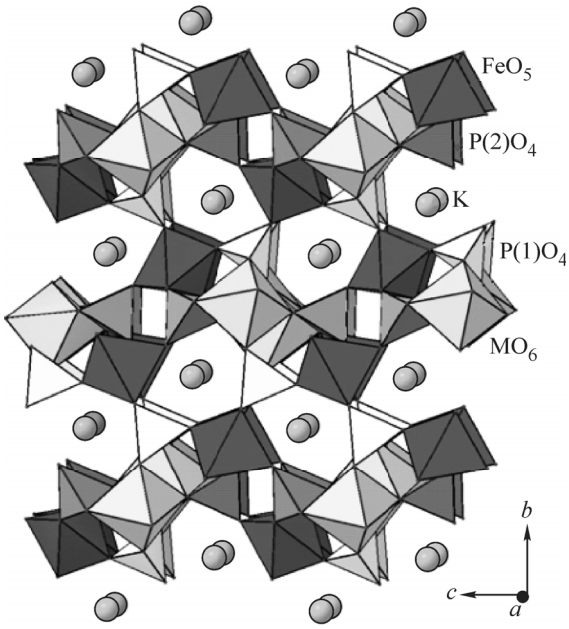

Fig. 2. Projection of the $KMFe(PO_4)_2$ structure on the (100) plane

data@fiz-karlsruhe.de, http://www.fiz-karlsruhe.de/request_for_deposited_data.html) on quoting CSD numbers 425924, 426857 and 426727.

Characterization. The experiments were carried out on a powder sample for KNi and on ground crystal samples for KMg-LT and KCo-LT. Thermal analysis (DTA) was conducted using a SETERAM 92 apparatus from 50 °C to 1100 °C by heating in the air atmosphere at a rate of 5 °C/min. The IR spectra were recorded in the wavenumber range 1800—400 cm^{-1} using a Perkin Elmer Paragon 1000 PC Fourier spectrometer.

RESULTS AND DISCUSSION

Structure description. All the title compounds are isostructural and display a new type of the framework made by a three-dimensional assemblage of MO_6 (M = Ni, Mg, Co) octahedra, FeO_5 trigonal bipyramids, and PO_4 tetrahedra (Fig. 2). Each MO_6 octahedron shares two opposite edges with two equivalent octahedra giving rise to infinite zigzag chains that run along the [100] direction (Fig. 3). The connection of these chains is ensured by the FeO_5 polyhedra and PO_4 tetrahedra leading to a 3D covalent framework with crossing tunnels parallel to the [100] and [001] directions where the potassium ions are located.

Fig. 4 shows the environments of the coordination polyhedra within the title structures. Each MO_6 octahedron shares two opposite edges with two equivalent octahedra. Additionally, it is linked to one FeO_5 polyhedron and four PO_4 tetrahedra through corner sharing and to one PO_4 tetrahedron via edge sharing. Each FeO_5 trigonal bipyramid shares four corners with four PO_4 tetrahedra, the fifth corner being doubly shared by one PO_4 tetrahedron and one MO_6 octahedron. The PO_4 tetrahedra are of two types labeled $P(1)O_4$ and $P(2)O_4$. Each $P(1)O_4$ tetrahedron shares three corners (two with two FeO_5 polyhedra and one with one MO_6 octahedron), the forth corner being doubly shared by two MO_6 octahedra. Each $P(2)O_4$ tetrahedron shares one edge with one MO_6 octahedron and three corners with three FeO_5 polyhedra.

Main interatomic distances are given in Table 5. The MO_6 octahedron is very distorted due to the edge sharing with the $P(2)O_4$ tetrahedron. Indeed, the M—O distances are highly dispersed (2.014(2)—2.200(2) Å for KNi, 2.005(2)—2.234(2) Å for KMg-LT, and 2.007(2)—2.298(2) Å for KCo-LT) around their mean values of 2.090(2) Å, 2.105(1) Å, and 2.122(2) Å respectively. The latter values are close to those observed for the octahedral environment of M^{2+} ions in $M_3(PO_4)_2$ phosphates (2.074 Å for Ni [15], 2.120 Å for Mg [16], 2.142 Å for Co [17]). The FeO_5 polyhedron is also highly distorted in view of the great discrepancy of Fe—O distances, varying between 1.891(2)—2.012(2) Å for KNi, 1.898(2)—2.013(2) Å for KMg-LT, and 1.892(2)—2.001(2) Å for KCo-LT. The correspondding mean distances of 1.934(1) Å, 1.939(1) Å, and 1.934(1) Å are consistent with 1.947 Å, observed for five-coordinated Fe^{3+} ions in $NaCaFe_3(PO_4)_4$ [18]. The mean P—O distances within the PO_4 tetrahedra are in the ranges 1.534(1)—1.538(2) Å for P(1) and 1.534(1)—1.537(2) Å for P(2). These values are close to 1.537 Å reported by Baur for the monophosphate groups [19]. The K^+ cations occupy a single type site located at the inter-

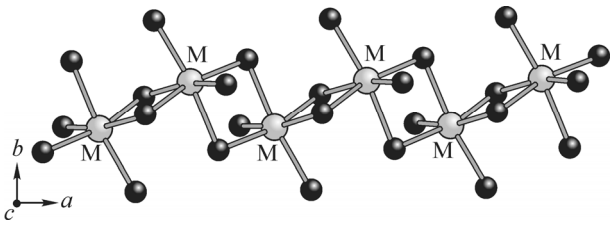

Fig. 3. Infinite chain of edge-sharing MO_6 octahedra

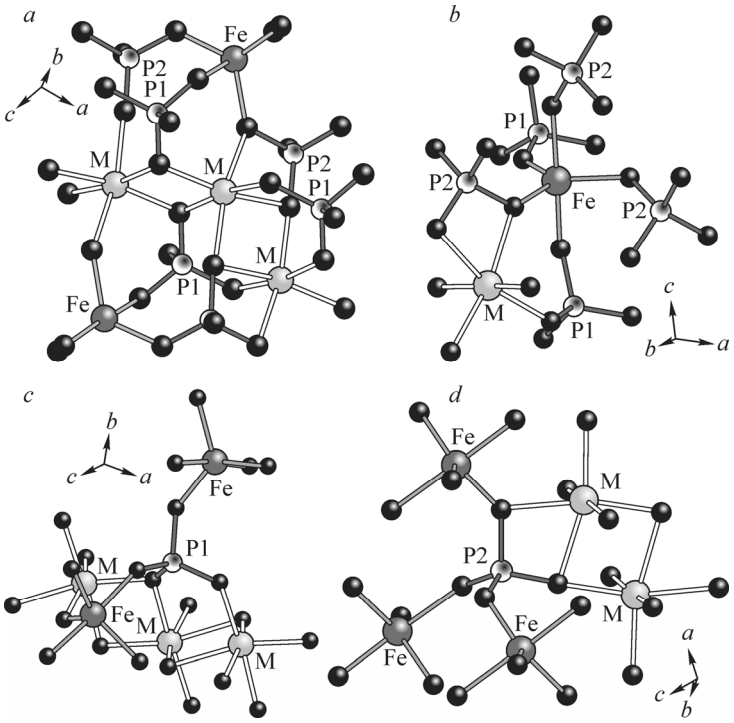

Fig. 4. Environments of the MO_6 (*a*), FeO_5 (*b*), $P(1)O_4$ (*c*), and $P(2)O_4$ (*d*) polyhedra in $KMFe(PO_4)_2$

Table 5

Selected bond lengths (Å) *for* $KMFe(PO_4)_2$ (M = Ni, Mg *and* Co)

Polyhedra		KNi	KMg-m	KCo-m	Polyhedra		KNi	KMg-m	KCo-m
MO_6	M—O14	2.014(2)	2.005(2)	2.007(2)	$P(2)O_4$	P(2)—O24	1.523(2)	1.522(2)	1.518(3)
	M—O13	2.024(2)	2.022(2)	2.053(2)		P(2)—O21	1.524(2)	1.525(2)	1.519(3)
	M—O13	2.072(2)	2.129(2)	2.096(2)		P(2)—O23	1.535(2)	1.534(2)	1.534(2)
	M—O21	2.079(2)	2.042(2)	2.101(2)		P(2)—O22	1.569(2)	1.564(2)	1.566(2)
	M—O22	2.149(2)	2.195(2)	2.179(2)		**⟨P(2)—O⟩**	**1.537(2)**	**1.536(1)**	**1.534(1)**
	M—O21	2.200(2)	2.234(2)	2.298(2)		**BVS**	**4.96**	**4.98**	**5.00**
	⟨M—O⟩	**2.090(2)**	**2.105(2)**	**2.122(2)**					
	BVS	**1.88**	**2.02**	**1.93**					
FeO_5	Fe—O11	1.891(2)	1.898(2)	1.892(2)	KO_n	K—O11	2.742(2)	2.767(2)	2.766(2)
	Fe—O23	1.918(2)	1.925(2)	1.918(2)	(n = 8 and 9)	K—O24	2.853(2)	2.823(2)	2.828(2)
	Fe—O12	1.923(2)	1.927(2)	1.927(2)		K—O23	2.855(2)	2.844(1)	2.832(2)
	Fe—O22	1.925(2)	1.932(2)	1.930(2)		K—O14	2.865(2)	2.851(2)	2.860(2)
	Fe—O24	2.012(2)	2.013(2)	2.001(2)		K—O12	2.898(2)	2.853(2)	2.870(2)
	⟨Fe—O⟩	**1.934(2)**	**1.939(1)**	**1.934(1)**		K—O13	2.915(2)	2.971(2)	2.933(2)
	BVS	**3.13**	**3.09**	**3.13**		K—O11	3.189(2)	3.101(2)	3.163(2)
$P(1)O_4$	P(1)—O14	1.520(2)	1.517(2)	1.518(2)		K—O24	3.210(2)	3.275(3)	3.250(2)
	P(1)—O12	1.528(2)	1.532(2)	1.525(1)		K—O21	3.279(2)	—	3.282(2)
	P(1)—O11	1.544(2)	1.547(2)	1.541(2)		**BVS**	**1.01**	**1.02**	**1.03**
	P(1)—O13	1.559(2)	1.553(2)	1.552(2)					
	⟨P(1)—O⟩	**1.538(2)**	**1.537(1)**	**1.534(1)**					
	BVS	**4.96**	**4.96**	**5.01**					

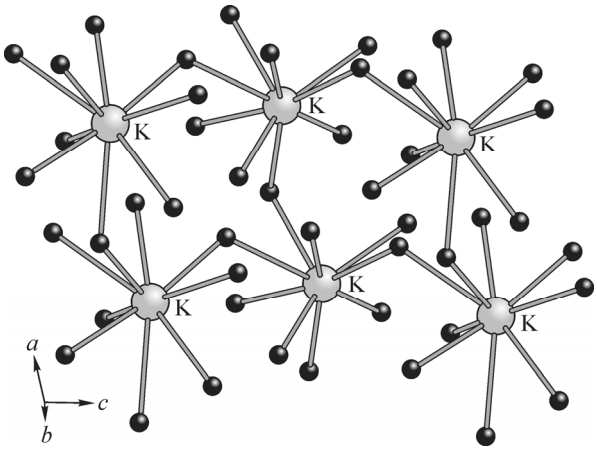

Fig. 5. Linkage of KO_9 polyhedra

section of the crossing tunnels. Their environment was determined by assigning K—O distances below $L_{max} = 3.33$ Å, as suggested by Donnay and Allmann [20]. It is formed by nine oxygen atoms with K—O distances in the range 2.742(2)—3.279(2) Å for KNi and 2.766(2)—3.282(2) Å for KCo-LT. In KMg-LT, the environment of K^+ ions is slightly different since it only has eight oxygen atoms with K—O distances varying between 2.767(2) Å and 3.275(3) Å. The KO_n ($n = 8$ and 9) polyhedra are corner-sharing to form chains in the *a*, *c* plane (Fig. 5).

The bond valence sums (BVSs) (Table 5) calculated by the Brown and Altermatt method [21] ($S = \exp[(Ri - di)/0.37]$, $R(K^+—O) = 2.132$ Å; $R(Ni^{2+}—O) = 1.654$ Å; $R(Mg^{2+}—O) = 1.693$ Å; $R(Co^{2+}—O) = 1.692$ Å and $R(P^{5+}—O) = 1.617$ Å) are in agreement with the formal charges deduced from the chemical formula.

Thermal study. **KNi.** The DTA curve in Fig. 6, *a* shows only one endothermal peak at 941 °C, indicating that for this compound no phase transition happens. The observed peak is attributed to the congruent melting of the product.

KMg-LT and KCo-LT. The DTA curves for the KMg-LT and KCo-LT compounds are shown in Figs. 6, *b* and 6, *c* respectively. These curves are very similar, consisting of two endothermic peaks at 778 °C and 914 °C for KMg-LT and at 840 °C and 883 °C for KCo-LT. This result was taken as an indication of a possible phase transition. An XRD pattern was measured for each compound after melting in a furnace at 950 °C and quenching to room temperature (Figs. 7. *a*, *b*). For KMg-LT, the analysis of the XRD pattern shows that the molten product exhibits the high-temperature lamellar structure previously reported for $KMgFe(PO_4)_2$ (monoclinic: $C2/c$; $a = 18.529(7)$ Å; $b = 5.402(3)$ Å; $c = 9.374(9)$ Å; $\beta = 120.64(5)°$) [7]. Thus, the $KMgFe(PO_4)_2$ low-temperature stable phase undergoes an irreversible phase transition at 778 °C. For KCo-LT, the XRD pattern of the molten product shows that it is isotypic with $KCoAl(PO_4)_2$ (monoclinic: $C2/c$; $a = 13.3179(15)$ Å; $b = 13.152(2)$ Å; $c = 8.683(2)$ Å and $\beta = 100.19(1)°$) [12], indicating an irreversible phase transition at 840 °C.

IR *spectroscopy.* The IR spectra of the title compounds (Fig. 8) show a strong absorption below 1500 cm^{-1} which is typical of monophosphate [22, 23]. According to the factor analysis, nine vibrational modes are expected for the PO_4 group [24]. The assignments are summarized in Table 6. The observed bands in the wavenumber ranges 1240—1030 cm^{-1} and 1030—900 cm^{-1} are attributed to asymmetric triply degenerate (ν_3) and symmetric P—O stretching (ν_1) modes respectively. The asymmetric triply degenerate (ν_4) and symmetric doubly degenerate (ν_2) of O—P—O bending modes are

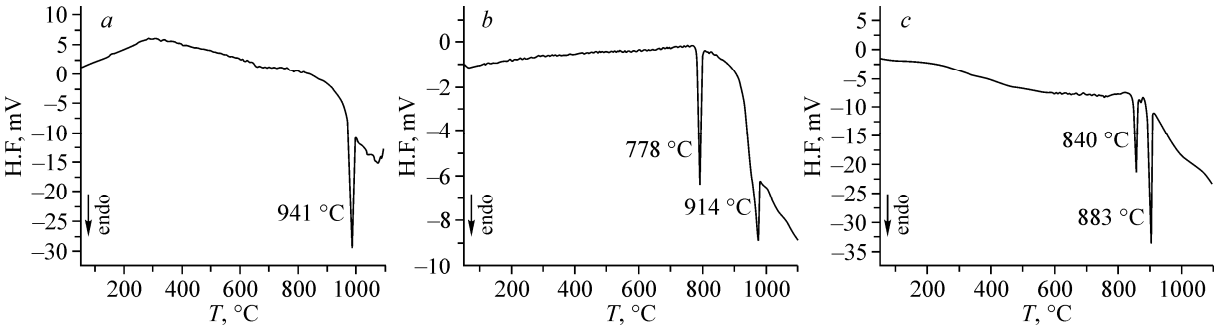

Fig. 6. DTA curve of $KNiFe(PO_4)_2$ (*a*), $KMgFe(PO_4)_2$ (*b*) and $KCoFe(PO_4)_2$ (*c*)

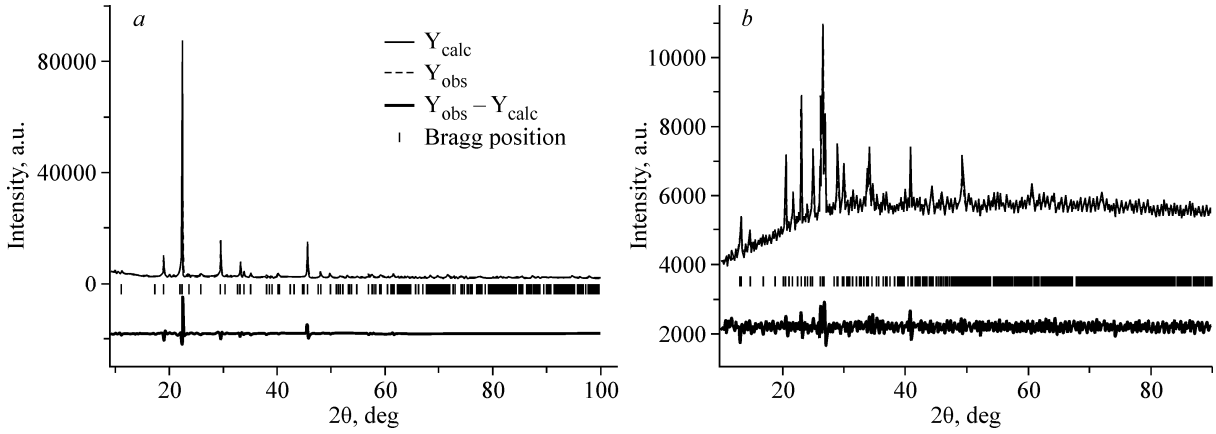

Fig. 7. XRD pattern of $KMgFe(PO_4)_2$ after melting and quenching to room temperature (*a*) and melting product of $KCoFe(PO_4)_2$ (*b*)

observed at 670—530 cm^{-1} and 470—400 cm^{-1} respectively. The occurrence of two distinct symmetric stretching bands (ν_1) in the range 1015—900 cm^{-1} with a large splitting indicates that there are two distinct PO_4 tetrahedra in each compound. The large width of the absorption bands observed below 680 cm^{-1} reflects the overlap with those corresponding to the vibration of M—O bonds.

From a comparison of the spectra, one can deduce that those of KCo-LT and KNi are similar in wavenumber, but a slight increase is observed for KMg-LT. This fact can be attributed to the ionicity of the M—O bond. In fact, the Mg—O bond is significantly more ionic than the Co—O and Ni—O bonds having nearly the same ionicity, leading to more covalent P—O bonds, and therefore the highest wavenumber for the KMg-LT compound.

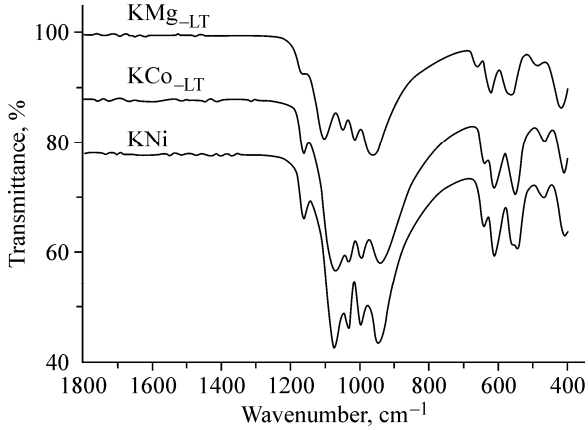

Fig. 8. IR spectra of $KMFe(PO_4)_2$ (M = Mg, Co, Ni)

CONCLUSIONS

Iron phosphates $KMFe(PO_4)_2$ (M = Ni, Mg, Co) were synthesized using the flux method with the atomic ratio *P*: Mo = 2:1 for KNi and KCo-LT and 2:2 for KMg-LT. Their crystal X-ray diffraction revealed that the three compounds were isostructural and exhibited a 3D framework made up by chains of edge-sharing MO_6 octahedra connected through the FeO_5 polyhedra and PO_4 tetrahedra, the K^+ ions being located in the intersecting tunnels. The thermal study showed a congruent melting of

Table 6

Assignment of IR absorption bands to different vibrations of the PO_4 *tetrahedra for* $KMFe(PO_4)_2$ (M = Ni, Mg *and* Co)

Compound	υ_{asy} (υ_3) (P—O)	υ_{sym} (υ_1) (P—O)	δ_{asy} (υ_4) (O—P—O)	δ_{sym} (υ_2) (O—P—O)
KNi	1161, 1074, 1034	997, 947	642, 612, 549	470, 409
KMg-m	1168, 1104, 1049	1015, 964	661, 624, 567	488, 418
KCo-m	1162, 1072, 1033	995, 942	640, 613, 550	469, 410

KNi at 941 °C and an irreversible phase transition from the low- to the high-temperature stable phases at 778 °C and 840 °C for KMg-LT and KCo-LT respectively. These results were confirmed by the analysis of the XRD patterns of their molten products. The IR spectra were consistent with the crystal structure, showing the presence of two different phosphate groups.

This work is supported by the AECID (Spain) and the DGRST (Tunisia), Project (Spain-Tunisia) (AP/036271/11).

REFERENCES

1. *Ai M., Ohdan K.* // Appl. Catal. A. – 1999. – **180**. – P. 47.
2. *McCormick R.L., Alptekin G.O.* // Catal. Today. – 2000. – **55**. – P. 269.
3. *Padhi A.K., Nanjundaswamy K.S., Goodenough J.B.* // J. Electrochem. Soc. – 1997. – **144**. – P. 1188.
4. *Massa W.* Crystal Structure Determination, 2nd ed. – Berlin, Heidelberg: Springer-Verlag, 2004.
5. *Maspoch D., Ruiz-Molina D., Veciana J.* // Chem. Soc. Rev. – 2007. – **36**. – P. 770.
6. *Riou-Cavellec M., Riou D., Ferey G.* // Inorg. Chim. Acta. – 1999. – **291**. – P. 317.
7. *Badri A., Hidouri M., López M.L., Veiga M.L., Wattiaux A., Ben Amara M.* // Solid State Ion. – 2009. – **180**. – P. 1558.
8. *Badri A., Hidouri M., López M.L., Pico C., Wattiaux A., Ben Amara M.* // J. Solid State Chem. – 2011. – **184**. – P. 937.
9. *Yatskin M.M., Zatovsky I.V., Baumer V.N., Ogorodnyk I.V., Slobodyanik N.S.* // Acta Crystallogr. – 1997. – **E68**. – P. i51.
10. *Yatskin M.M., Zatovsky I.V., Strutynska N.Yu., Baumer V.N., Slobodyanik N.S.* International Conference on Oxide Materials for Electronic Engineering OMEE, 2012.
11. *Yakubovich O.V., Evdokimova O.A., Mel'nikov O.K., Simonov M.A.* // Kristallografiya. – 1986. – **31**. – P. 906.
12. *Chen X.-A., Zhao L., Li Y., Guo F., Chen B.-M.* // Acta Crystallogr. – 1997. – **C53**. – P. 1754.
13. *Altomare A., Cascarano G., Giacovazzo C., Guagliardi A.* // J. Appl. Crystallogr. – 1993. – **26**. – P. 43.
14. *Sheldrick G.M.* SHELX-97, Release 97-2. – Germany, University of Göttingen, 1998.
15. *Calvo C., Faggiani R.* // Canad. J. Chem. – 1975. – **53**. – P. 1516.
16. *Nord A.G., Stefanidis T.* // Acta Chem. Scand. – 1968. – **22**. – P. 1466.
17. *Nord A.G., Stefanidis T.* // Acta Chem. Scand. – 1983. – **A37**. – P. 715.
18. *Hidouri M., Lajmi B., Wattiaux A., Foures L., Darriet J., Ben Amara M.* // J. Alloys Compd. – 2003. – **358**. – P. 36.
19. *Baur W.H.* // Acta Crystallogr. – 1974. – **B30**. – P. 1195.
20. *Donnay D., Allmann R.* // Am. Mineral. – 1970. – **55**. – P. 1003.
21. *Brown I.D., Altermatt D.* // Acta Crystallogr. – 1985. – **B41**. – P. 244.
22. *Benarafa L., Rghioui L., Nejjar R., Idrissi M.S., Knidiri M., Lorriaux A., Wallart F.* // Spectrochim. Acta. – 2005. – **A61**. – P. 419.
23. *Tomaszewski P.E., Maczka M., Majchrowski A., Waśkowska A., Hanuza J.* // Solid State Sci. – 2005. – **7**. – P. 1201.
24. *Müller A., Krebs B.* // J. Mol. Spectrosc. – 1967. – **24**. – P. 180.